Understanding the Value of Comprehensive Material, Performance Models and Real Failure Modes in Modern Rigid Pavement Designs

Juan Pablo Covarrubias, Pelayo Del Rio, Dr. Feng Mu, Sherry Sullivan

Abstract

Rigid pavements traditionally have been designed using either empirical or mechanistic-empirical methodologies. Historically, common design methods included AASHTO (1993 and 2008) and the PCA Method (now known as Street Pave or Pavement Designer). These design methods were calibrated using a relatively limited number of pavements with slab dimensions of 12ft (3.5m) wide and 15ft (4.5m) long, different traffic levels, local climate conditions and materials and construction practices from the era of the testing. In addition to these methods, modern methods including bonded and unbonded concrete overlays and slabs with optimized geometry are becoming increasingly common.

While historical methods might provide appropriate designs for certain geometries (slabs sizes), applications and locations like those to which they were calibrated, the appropriateness of their application should be in question (e.g., AASHTO 93's limit of testing to a certain amount of ESALs and climatic conditions). Mechanistic performance methods allow the incorporation of new materials and conditions, but understanding the mechanistic principle that the method is trying to extrapolate and the resulting failure mode of this new condition is an important consideration.

This paper contrasts historical and modern rigid pavement design methods and their results, with an emphasis on illustrating when historical designs might yield unconservative and possibly dangerous or incorrect designs because of their lack of consideration of comprehensive performance models.

Rigid Pavement Design Empirical Methods

AASHTO 93. The AASHTO method is based on the 1950's AASHO Road Test. This test was the first source of experimental data associated with the damage caused by vehicles on a pavement. For two years, heavy vehicles with a range of loads, drove across the test sections until loss of serviceability was recorded. A maximum of 1,114,000 axle applications was achieved, translating to 8 million equivalent single axle loads (ESALs) on the most highly trafficked sections. The transverse joint spacing of the pavement was 15ft (4.5m). Loss of serviceability was first reported on the slabs with 40ft (12m) joint spacing, with transverse cracks every 12ft to 15ft (3.6m to 4.5m). Therefore, the AASHTO method equations are based on slabs with joints spaced at 15ft to 20ft (4.5m to 6m).

The scope of the AASHTO equations is defined by the specific range in which the slabs are loaded. If the failure mode of the slabs change per the loads being applied in a different way, the equations of the method are outside the calibrated range. With a joint spacing of 15ft (4.5m), the truck's front axle and first rear one will be within a same slab in any given time.

Figure 1, Traditional slab dimension

Significant stresses occur on the top of a slab when the curled edges are loaded. This is the case on any slab with dimensions that allow both axles to be on the same slab simultaneously. If a pavement is designed with a joint spacing other than the 15ft (4.5m) recommended by AASHTO, it could be outside the range of the method, since the condition in which the slabs are loaded is conceptually different.

Another important point about the AASHTO method is the equation used to calculate permissible traffic per serviceability in concrete pavements:

$$log_{10}(W_{18}) = Z_R \times S_0 + 7{,}35 \times log_{10}(D+1) - 0{,}06 + \frac{log_{10}\left[\frac{\Delta PSI}{4{,}5-1{,}5}\right]}{1+\frac{1{,}624\times 10^7}{(D+1)^{8{,}46}}} + (4{,}22 - 0{,}32 \times p_t) \times log_{10}\left[\frac{S_c' \times C_d \times (D^{0{,}75}-1.132)}{215{,}63 \times J\left[D^{0{,}75}-\frac{18{,}42}{(E_c/k)^{0{,}25}}\right]}\right] \quad (1)$$

Basic design equation for rigid pavements, AASHTO 93, page I-6

This equation results in the permissible traffic, expressed as "W_{18}". The input values involved are statistical factors (Z_R and S_0), pavement thickness (D), loss of serviceability (Δ PSI) and local calibration factors.

The length of the slab does not affect this equation since there is a standard joint spacing of 15ft (4.5m). Joint spacing is not an input or an output value in this method. The only parameters that can be varied to obtain an expected serviceability are pavement thickness and the load transfer efficiency (J). These parameters, regardless of local calibration parameters, are correlated with the permissible traffic so that the permissible traffic will increase if the thickness increases or the load transfer efficiency decreases, and vice versa.

Therefore, in the AASHTO 93 method, pavement thickness is an input, not an output, and it is not related to joint spacing.

Rigid Pavement Design Mechanical Methods

PCA. The PCA methodology (1984), unlike the AASHTO methodology of that time, is a mechanistic methodology, with fatigue equations based on concrete beams tested for flexural strength, calibrated by several road and laboratory tests. Its main equation relates pavement stresses with slab thickness, and the relative rigidity radius between the slab and the subgrade, which is a function of the concrete properties and the ground. In addition, it includes different adaptations and calibration constants per design criteria for different cases.

$$\sigma_{eq} = \frac{M_e}{h^2} * f_1 * f_2 * f_3 * f_4 \quad (2)$$

Where:

M_e = $\begin{cases} -1600 + 2525\log(l) + 24.42l + 0.204l^2 \ ) & (for\ single\ axles\ with\ no\ edge\ support) \\ -3029 + 2966.8\log(l) + 133.69l - 0.0632l^2 & (for\ tandem\ axles\ with\ no\ edge\ support) \\ (-970.4 + 1202.6 * \log[l] + 53.587l) * (0.8742 + 0.01088 * k^{0.447}) & (for\ single\ axles\ with\ edge\ support) \\ (-2005.4 + 1980.9 * \log[l] + 99.008l) * (0.8742 + 0.01088 * k^{0.447}) & (for\ tandem\ axles\ with\ edge\ support) \end{cases}$

σ_{eq} = $equivalent\ stress, psi$

l = $radius\ of\ relative\ stiffness\ of\ the\ slab - subgrade\ system$

E = $modulus\ of\ elasticity, psi$

μ = $Poisson's\ ratio\ for\ concrete$

h = $slab\ thickness, in$

k = $modulus\ of\ subgrade\ reaction$

f_1 = $adjustment\ factor\ for\ the\ effect\ of\ axle\ loads\ and\ contact\ area$

f_2 = adjustment factor for a slab with no concrete shoulder (based on analysis conducted using PCA-MATS computer program (MATS, 1990)

f_3 = $adjustment\ factor\ to\ account\ for\ the\ effect\ of\ truck\ (wheel)\ placement\ at\ the\ slab\ edge\ on\ edge\ stress$

l = $adjustment\ factor\ to\ account\ for\ increase\ in\ portland\ cement\ concrete$

The failure mode for this method is transverse cracking and erosion under the joints. Cracking is calculated only from the bottom up and with the load at the edge of the slab, incorporating stabilized bases and edge type. Erosion can be mitigated by increasing the slab thickness, using dowels and a tied PCC shoulder.

Over time, this methodology derived into a software called StreetPave12 and more recently, an online software called Pavement Designer. These predict the percentage of cracked slabs and the magnitude of the erosion of the base.

Since this approach, founded on PCA, is simplistic, there are some limitations. Such as the exclusion of slabs curling/deformation, slab dimensions as an input, the possibility of calculating top-bottom stresses, among others. Also, the PCA methodology has fatigue equations based on the results of a flexural test on concrete beams with third-point loading, which behaves in a different way to a slab on ground.

AASHTO 2008 (Pavement ME). The most advanced methods currently available for evaluating and designing JPCP and CRCP pavements are AASHTO 2008 or Pavement ME.

It focuses on estimating responses based on results obtained by finite elements analysis, considering the accumulation of fatigue and faulting hour-to-hour throughout the entire pavement life, using parameters calibrated empirically with more than 2,500 test sections.

The number of loads allowed for a condition in AASSHTO 2008 is calculated through a function that relates the concrete module of rupture with the stress in the slabs as shown in the following equation:

$$Log(N) = 2 * \left(\frac{M_r}{\sigma_{total}}\right)^{1.22} \quad (3)$$

$$Fatigue = \sum_i \sum_j \sum_k \sum_l \sum_m \sum_n \frac{n_{ijklmn}}{N_{ijklmn}} \quad (4)$$

Where:

n_{ijklm} = $number\ of\ loads\ applied\ in\ the\ condition\ i, j, k, l, m, n$
N_{ijklm} = $number\ of\ possible\ loads\ in\ the\ condition\ i, j, k, l, m, n$
i = $year$
j = $season$
k = $axle\ combination$
l = $load\ level$
m = $temperature\ gradient$
n = $traffic\ path$

Cracking is calculated from top-bottom and bottom-top stresses, always at the edge of the slab. In addition, it can calculate joint faulting and IRI accurately over time by using an energy differential model at the joint.

Although it is considered as the most accurate software for estimating the behavior of rigid pavements, it also has some limitations. As in the methods described above, its application in terms of slab dimensions is restricted to a minimum joint spacing of 3 meters long, because this was the calibration limit and corresponds to the loading mode in slabs with traditional dimensions.

OptiPave. This methodology, based on the same equations as Pavement ME, corresponds to a software developed and calibrated to design thin concrete pavements with optimized geometry, which means slabs with dimensions such that they can never be loaded by more than one wheel or set of wheels of a truck at the same time. It is the only methodology capable to design with precision concrete pavements with joint spacing less than 2.5 meters long. Like AASHTO 2008, it is founded on the calculation of stresses using neural networks based on ISLAB2000, integrating an accumulated fatigue equation as used in Pavement ME. This mechanistic-empirical methodology was calibrated using real scale tests and has been updated with information of different projects with this technology.

The software predicts the total percentage of cracked slabs, adding transverse, longitudinal and corner cracks at 3 different points of the slab for each failure mode due to cracking. It also calculates faulting and IRI year to year in slabs of small dimensions to reduce the effects of the interaction between curling and load stresses.

The number of admissible load repetitions is a function of the concrete's stress and strength, per the following equation:

$$log(N_{i,j,k,l}) = 2 * \left(\frac{\sigma_{i,j,k,l}}{MOR * C_1 * C_2}\right)^{-1.22} \quad (5)$$

Where:

N_{ijkl} = $number\ of\ possible\ loads\ in\ the\ condition\ i,j,k,l$
σ_{ijkl} = $stress\ for\ condition\ i,j,k,l$
MOR = $module\ of\ rupture$
C_1 = $fracture\ mode\ factor: C_1 = a * h_{pcc}^2 + b * h_{pcc} + c$
h_{pcc} = $concrete\ thickness$
C_2 = $structural\ fiber\ factor: C_2 = \frac{f_{150}^{150}}{MOR} * SF * a$
a,b,c = $calibration\ factors$

The percentage of cracked slabs is calculated using the same model used in AASHTO 2008 and the fatigue damage is obtained per the relation between the number of real load repetitions and the number of admissible load repetitions. The calibration includes concrete pavements with thicknesses between 3in to10in (8cm to 25cm), with plain concrete and fiber reinforced concrete.

Among its limitations, OptiPave has more restrictive input values than Pavement ME, a restrictive set of data for calibration, due to the short time that the technology has being used, and finally that this methodology is only suitable for designing slabs of less than 8ft (2.5m) long.

Fiber reinforced concrete (FRC)

The structural fiber (steel or synthetic) allows the concrete to be more ductile (for small controlled deformations) and more controlled in terms of cracking propagation, this improves the load capacity of the slab, the fatigue resistance and durability of the pavement. Further, it provides the capability to resist non–homogeneous platforms, and after cracking occurs, it holds the crack together extending the afterlife of the pavement.

Two types of behavior can be observed in flexural tests using concrete beams: first, with high fiber doses (enough to increase flexural strength after the first crack) and the second, with low fiber doses (such that once the first crack in the concrete beam occurs), there is a decrease in the load capacity towards a percentage of the flexural concrete strength (residual strength).

This paper will focus on the second case mentioned, since it is the most efficient solution in terms of construction and usually cost. In this case, several advantages can be obtained adding low doses of fiber, including:

- Increased puncture capacity of the slab,
- Increase fatigue capacity for cyclical loads
- In the post-cracking stage of concrete, the fiber ties the concrete between fissures, avoiding fragile breakage and detachment of material.

Except in very high doses, adding fiber to concrete does not impact its flexural strength, since it works once the concrete is cracked. By measuring the flexural strength of a concrete beam using a standardized test, where the final strength of the concrete is recorded immediately before the beam fracture. Therefore, a greater displacement is required to completely fail the fiber reinforced specimens. (Residual Strength).

The graphs presented in Figure 2**¡Error! No se encuentra el origen de la referencia.** represents the results obtained from loading vs deformation for a round panel per ASTM C1550, for a standard beam per ASTM 1609, and for a slab over the ground, respectively. The results show that for low fiber doses, there is no increase in the concrete flexural strength and load capacity decreases immediately after the first crack that increases with deformation.

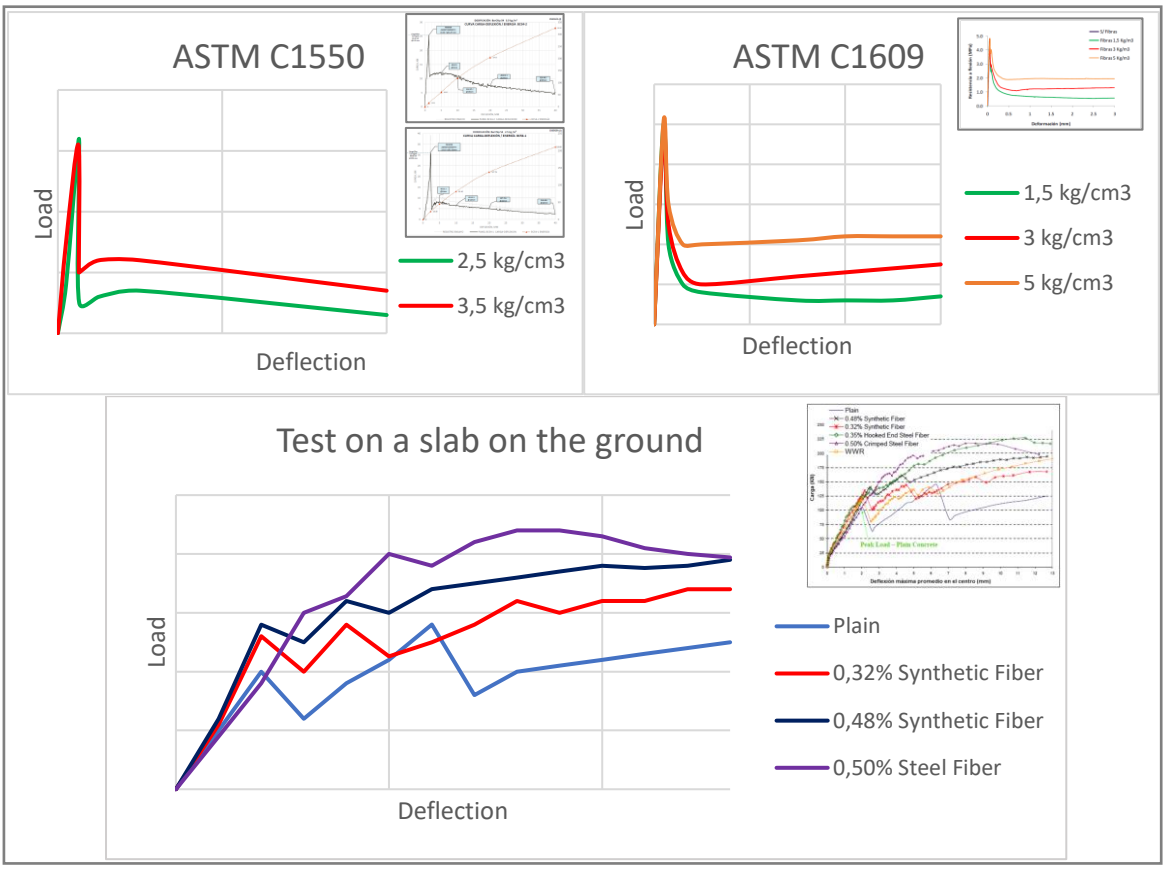

Figure 2, Schematic differences between test methods for flexural performance of FRC

Concrete pavement slab behavior

Possible Failure Modes. There are six possible failure modes that result from excessive load repetitions for concrete pavement slabs. These failure modes can occur independently and are dependent on the magnitude and location of the stresses and deformations in the slab. These failure modes are a function of the slab geometry, the environmental conditions, and the material properties. A schematic of the location and appearance of these six failure modes with respect to the traffic direction is given in Figure 3.

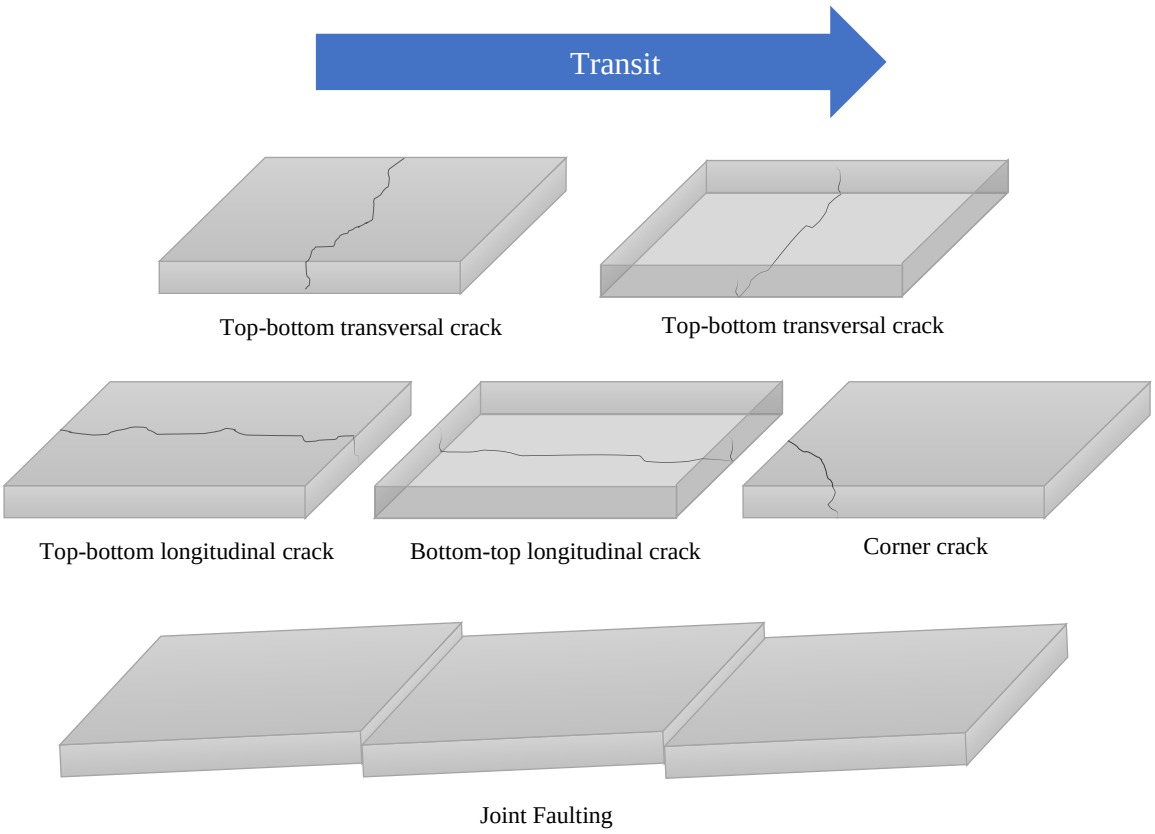

Figure 3, Possible failure modes

Built in Curling. Built-in curling (BIC) is permanent upward curvature of the concrete slab produced by irreversible moisture and temperature gradients between the top and the bottom of the slab. With mechanical loading, built-in curling typically changes the location and magnitude of the maximum tensile stress in the slab as larger regions of the slab lose contact with the support layer.

BIC in concrete pavements is a combination of five equivalent temperature components as shown in Equation 6. These factors are significantly affected by the local climate conditions, concrete mixture parameters, concrete properties, and construction techniques.

$$T_{tot} = T_{tg} + T_{mg} + T_{bi} + T_{shr} - T_{crp} \quad (6)$$

Where:

T_{tot} = Total effective linear temperature difference (TELTD)

T_{tg} = *Equivalent temperature difference between top and bottom of a slab due to the nonlinear temperature profile in the slab*

T_{mg} = *Equivalent temperature difference between top and bottom of a slab due to the nonlinear moisture gradient in the slab*

T_{bi} = *Equivalent temperature difference between top and bottom of a slab due to the nonlinear construction temperature profile built in to the slab*

T_{shr} = *Equivalent temperature difference between top and bottom of a slab due to the irreversible drying shrinkage between top of the slab and bottom of the slab*

T_{crp} = *Part of* T_{bi} *and* T_{shr} *recovered through tensile creep of the slab*

Field studies that have measured built in curling have shown values up to -66.6°F (-19.2°C) in Chile, -98.6°F (-37°C) in Pennsylvania, -41°F (-5°C) in Florida, or up to -104°F (-40°C) in the high mountains of Bolivia.

When this concave slab geometry is combined with traffic loading, critical top-down tensile stresses in the slab can result and, therefore, should be considered in the structural design of concrete pavements.

Current methods exist that calculate stresses for flat concrete slabs (without curling), and then superimpose stresses generated only by curling. Recent studies (Salsilli and PNA) have shown that this assumption is inaccurate, and the real stresses should be calculated by modeling curled slabs with full truck loading.

Behavior of the "Pavement System". As explained before, the failure mode experienced by the pavement can change and is dependent on the maximum load, slab thickness, fiber content, and the origin of the crack (top-bottom or bottom-top), among other factors.

The pavement structure should be interpreted not only as thickness, but as a "pavement system" or an integral system, (Michael Darter PhD M. " History and Future of Concrete pavement Design " at the 50th annual meeting ACPA).

A fatigue crack that develops from top to bottom in a pavement slab is normally produced when the slab is loaded simultaneously by more than one load. This type of crack begins at the free edge, without any restriction except the concrete strength, similarly to flexural strength tests of a beam. However, if the concrete were reinforced with fiber, it would be unable to resist large displacements (unless very high doses of fiber were used) which would therefore not provide structural contribution. However, if the fiber dose is sufficient to produce concrete hardening, the fiber could be considered to be contributing to the structural capacity.

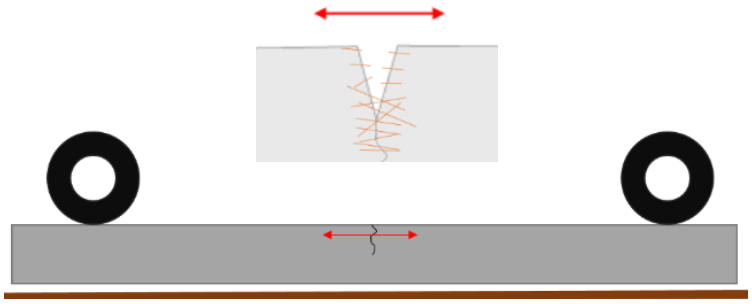

Figure 4, Top to bottom crack scheme with FRC

When the fatigue crack develops from bottom to top, the crack begins at the restricted edge because the base produces confinement that limits the opening and development of the crack. The friction with the base layer also directly affects vertical displacement, increasing the necessary energy for crack propagation.

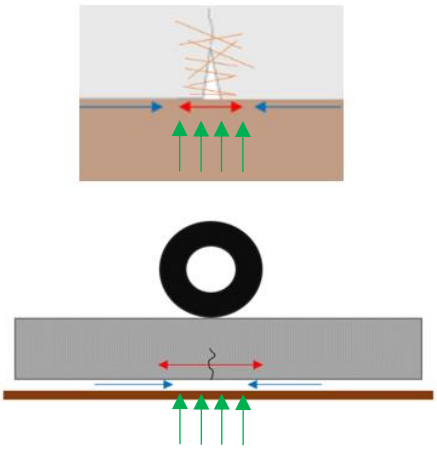

Figure 5, Bottom to top crack scheme with FRC

Due to the differences between top-down and bottom-up stresses, it was necessary to develop the "C_1" factor to reflect the interaction between the “pavement system” and loads when the tension predominates on the bottom face of the slab. This factor is close to 2 when the pavement is 3.1 in (8 cm) thick, and decreases to 1 when the slab thickness is increased as shown in Figure 6.

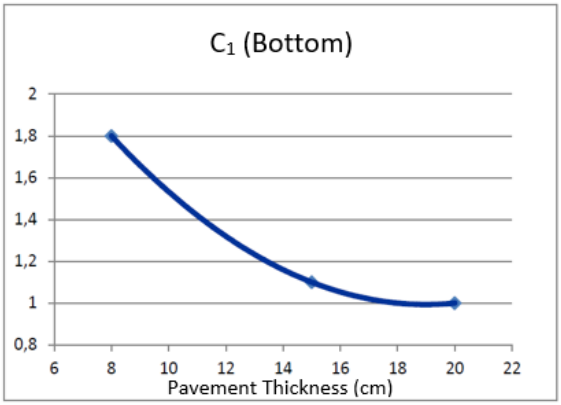

Figure 6, C1 factor vs Concrete thickness

In the case of using FRC in normal doses, the fiber also slows crack propagation. This prevents a sudden failure to the “pavement system” even if the material has a loss in capacity following the development of a crack.

With fiber, the system can withstand a higher load than plain concrete up to the first failure (Figure 2). Additionally, the loss in capacity following cracking is less severe, maintaining the structural capability of the slab while increasing the fatigue capacity of the “pavement system”.

It has been observed on multiple South American projects that top-down failure modes are the predominant failure mode under varied conditions. Therefore, utilizing methods that do not consider this failure mode can be dangerous as they are “blind” to some failure modes.

Research

Stress analysis. Pavement system behavior was analyzed by completing a study comparing stresses resulting from altering critical input variables. Loading was kept consistent and was simulated by placing a truck with a simple front axle and tandem rear axle on the concrete pavement. Additionally, the loading case of the single wheel load located at the edge of the pavement was modeled to simulate the calculation made by StreetPave.

Variables. The loads included in the analysis were placed to simulate typical truck loading on concrete pavement. All axles had a consistent wheelbase of 84 inches (213 cm), the front axle was separated by the tandem rear axle by 118 inches (300 cm), while the tandem axle had a between axle spacing of 59 inches (150 cm). The entire simulated truck weighed 46.3 kips (21,000 kg) with an evenly distributed weight. The entire loading scheme is given in Figure 8 below and the inputs values to generate the design scenarios are given in Table 1.

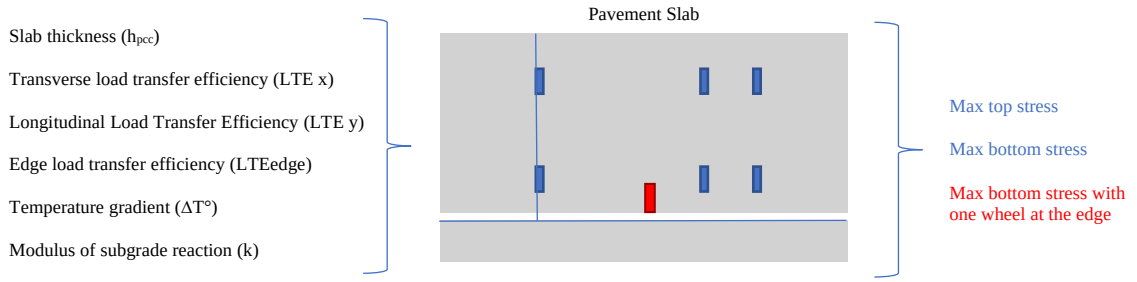

Figure 7, Research scheme

Table 1, Research variables

Joint spacing ft (cm)	**Slab thickness** In (cm)	**LTE x** (%)	**LTE y** (%)	**LTE edge** (%)	**ΔT°** °F (°C)	**K-value** Psi/in (kg/cm^3)
3.3 (100)	3.9 (10)	50	25	1	0 (0)	110 (3)
4.1 (125)	4.7 (12)		50	25	-9 (-5)	180 (5)
4.9 (150)	5.5 (14)		75	50	-18 (-10)	250 (7)
5.7 (175)	6.3 (16)		95		-27 (-15)	360 (10)
6.6 (200)	7.1 (18)				-36 (-20)	540 (15)
7.4 (225)	7.9 (20)					720 (20)
8.2 (250)	8.7 (22)					
9.8 (300)	9.4 (24)					
13.1 (400)						
16.4 (500)						

These scenarios were calculated using the finite element analysis software for rigid pavements ISLAB2000™, which allows for the calculation of stresses at specific locations on the pavement and always selects the maximum principal stress obtained at the top and bottom surface of the slab in each scenario.

The use of dowels was simulated by varying the load transfer efficiency (LTE) in transverse joints; lower LTE values were also included to study the effect of load transfer efficiency. The LTE at the edge was varied to simulate different edge types of a pavement and the temperature gradient (°ΔT) was used to represent the slab curvature (curling) and was

measured in degrees Celsius to indicate the temperature gradient that should be applied between the slab faces to eliminate the curvature.

Differences between top and bottom stress analysis. Under the standardized loading conditions, the maximum stresses on the top and bottom of the slabs occur in different locations across the slab face. The location of the maximum stresses itself is critical to completing the stress analysis for a pavement in response to each traffic loading scenario. The maximum stress on the top of the slab occurs when the slab is loaded between the edges. This maximum value often occurs under normal loading conditions and the deterioration potential of the slab under this loading scenario is indicated by the red areas in Figure 8. However, the bottom stress reaches its local maximum value immediately under the loads, regardless of slab dimensions. The distribution of the deterioration potential of the slabs is shown by the red area in Figure 8, below.

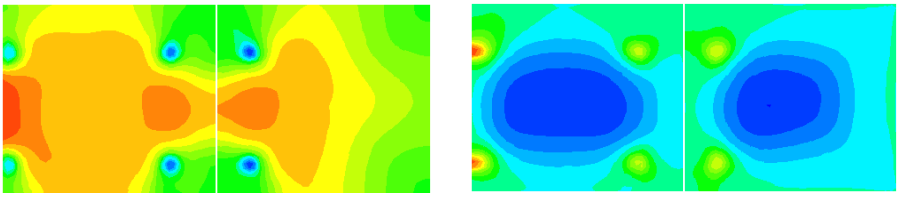

Figure 8, Slab top stress and Slab bottom stress

Results

Relationship between slab stresses and joint spacing First, the case of flat slabs will be discussed followed by the case of upwardly curled slabs. The resulting stresses across a spectrum of different joint spacing will be discussed for each slab type.

Case 1.1 (Flat slabs):

A slab is considered flat when the temperature gradient experienced by the slab is 0°F (0°C), meaning there is no resulting change of shape of the slab.

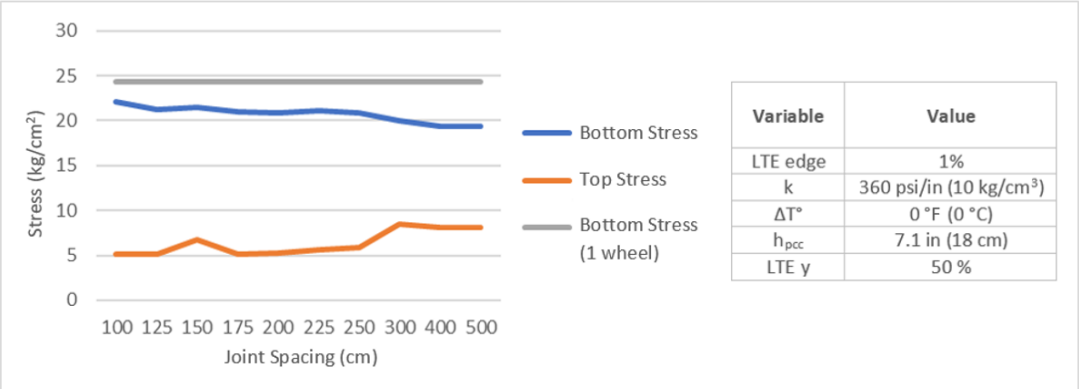

Variable	Value
LTE edge	1%
k	360 psi/in (10 kg/cm³)
ΔT°	0 °F (0 °C)
h_{pcc}	7.1 in (18 cm)
LTE y	50 %

Figure 9, Stresses vs joint spacing with flat slabs

Figure 9 shows the varying stresses calculated under the same loading configuration with different joint spacing. The three stresses plotted are the maximum stresses of each condition and position. It can be seen from Figure 9 that the stresses can vary as a function of the joint spacing. The maximum stress at the bottom of the slab ranged between 270 and

330 psi (19 and 23 kg/cm^2) while the average stress at the top of the slab ranged between 70 and 130 psi (5 and 9 kg/cm^2). The maximum stress at the slab bottom with one wheel remained constant and stable regardless of joint spacing but with an overall higher stress.

The analysis was then repeated while maintaining a constant joint spacing of 13 feet (4 m) and varying the slab thickness and k-value. All other input values remained unchanged. The results produced from this set of analyses is given in Figure 10.

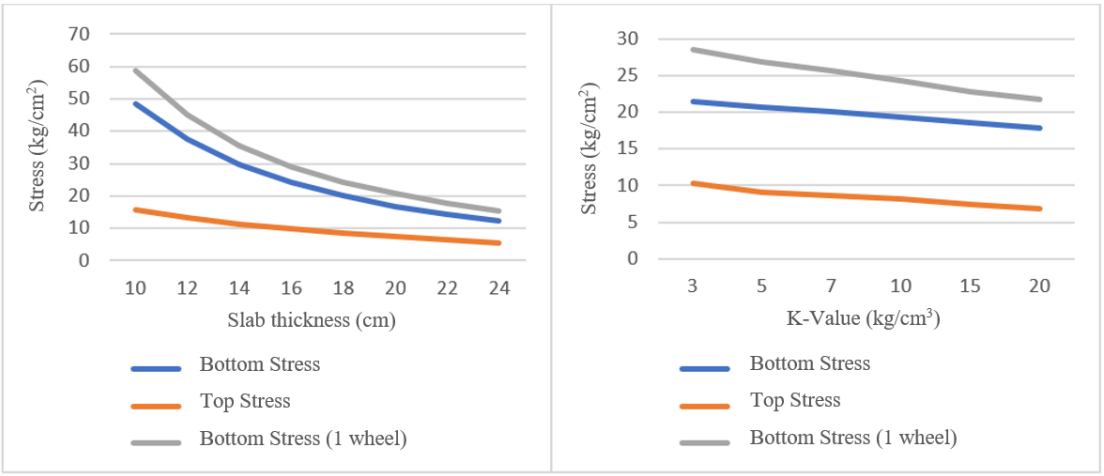

Figure 10, Stress vs Thickness and Stress vs K-value, flat slabs

It can be seen from Figure 10 that increasing the slab thickness substantially decreased the maximum stresses in the slab. This effect was most pronounced for the maximum stress across the bottom of the slab and the maximum stress across the bottom of the slab with only a single wheel loading. Also, it can be seen that the stress decreases evenly with the k-value across the three conditions of maximum stress. In this case of flat slabs, the maximum stress occurs at the bottom of the slab and this is the determining maximum stress for the system. This maximum stress location, or failure mode, being at the bottom and the edge (gray line) of the slab does not change with the slab geometry or rigidity of the subgrade support system in this examined case. However, this failure mode is unrealistic since slabs are often curled upward and exhibit different behavior.

Case 1.2 (Upward Curvature, Chile Case Study):

The second case of slabs considered are upwardly curled slabs. The slabs curl upward as a result of the temperature variation between each side of the slab, resulting in an internal temperature gradient. For this case, an internal temperature gradient of -27°F (-15°C) was used, considered to be a representative value experienced by pavements in Chile. All other parameters were kept constant to what was in the previous case and only the joint spacing was varied. The plot of the calculated stresses for varying joint spacing is given in Figure 11 below.

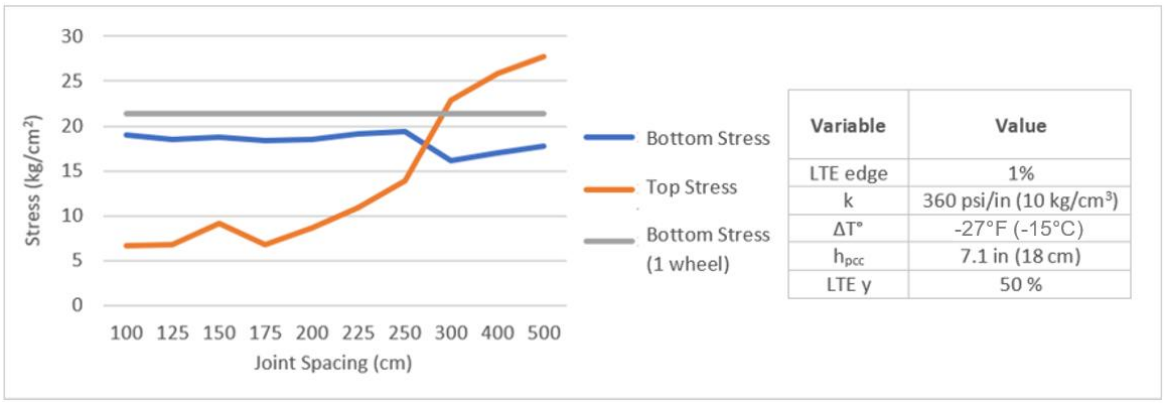

Variable	Value
LTE edge	1%
k	360 psi/in (10 kg/cm³)
ΔT°	-27°F (-15°C)
h_{pcc}	7.1 in (18 cm)
LTE y	50 %

Figure 11, Stress vs joint spacing, case in Chile

Unlike flat slabs, the location of the absolute maximum stress varies with joint spacing. As the joint spacing increases, the stresses on the top of the slab surpass the absolute value of the maximum stresses on the bottom of the slab. There is a substantial increase in the stresses on the top of the slab after the joint spacing exceeds 8.2 ft (250 cm). In addition, there is a local increase in the top stress when the joint spacing is 4.9 ft (150 cm). This slab length corresponds to the distance between the axles of the tandem axle, where there is an amplification of the maximum top stress when the slab is loaded on both edges.

The same analysis can be completed by holding the slab size consistently to 13 ft (4 m) across varying slab thicknesses between 3.9 and 9.4 inches (10 and 24 cm). All other design inputs were held constant and these results are given in the left graph in the Figure 12. Additionally, the thickness was then held consistent and the subgrade support conditions were varied, and these results are plotted in the right graph of the Figure 12.

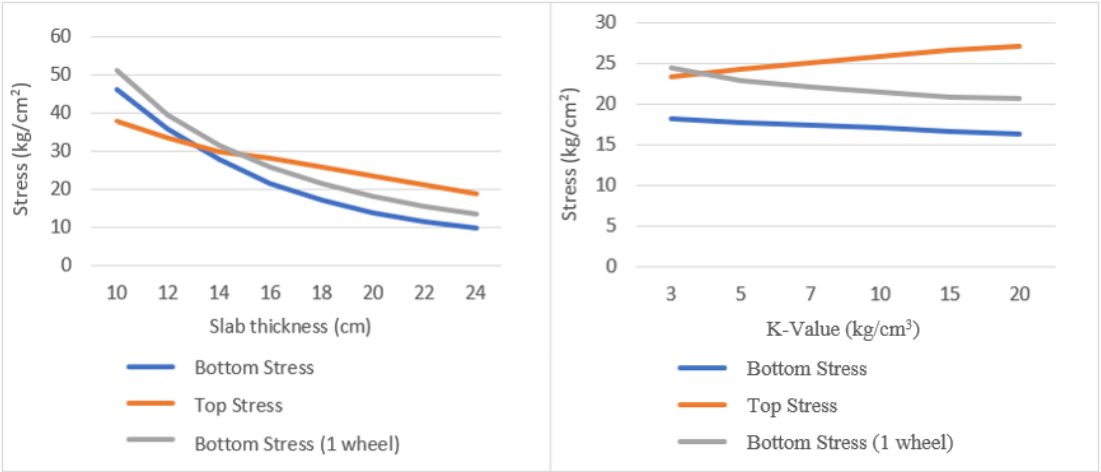

Figure 12, Stress vs Thickness and Stress vs K-value, case in Chile

Similar to Case 1.1 with flat slabs, the stress decreases while slab thickness increase. However, as seen in Figure 12, from 5.9 inches (15 cm) thick, the top stress prevails over the bottom stress as the maximum absolute stress. Additionally, Figure 12 shows that as the subgrade stiffness increases, the maximum stress occurs on the top of the slab. However, the conclusion that the maximum stress would occur on the top of the slab

directly conflicts with slab behavior predicted by previous models including the PCA or AASHTO 93 methods.

This analysis was repeated with a joint spacing of 5.7 ft (1.75 m) and the results are given in Figure 13.

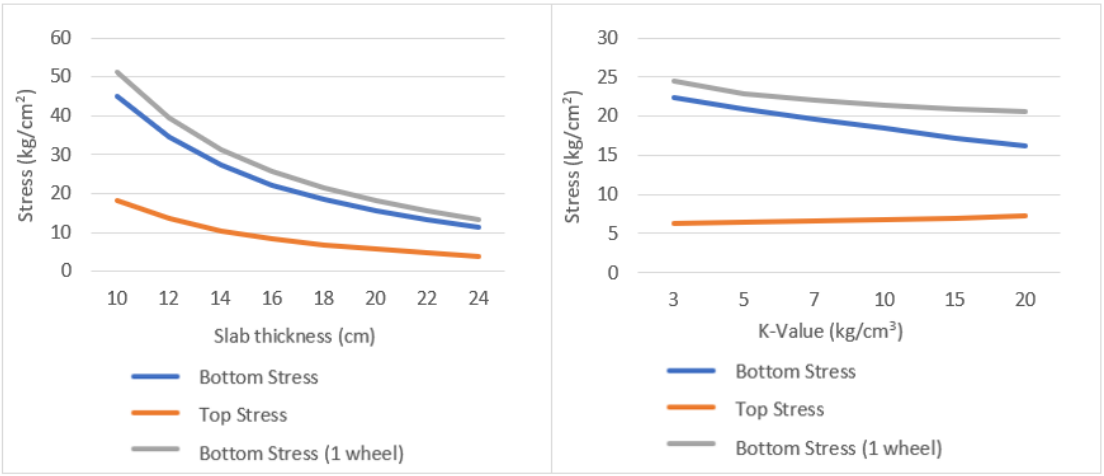

Figure 13 Stress vs Thickness and Stress vs k-value, short slabs

The lowered stresses, indicated in Figure 13, indicate that when slab size is reduced such that they can never be loaded by more than a single set of wheels, the top stress values does not control the design.

Finally, stress analyses were completed with two different joint spacing values (9.8 and 5.7 ft [4 and 1.75 m]), were held constant along with the remaining design input values while varying only the temperature gradient. The results of this analysis can be seen in Figure 14 for the larger 9.8 ft (4 m) joint spacing and for the smaller 5.7 ft (1.75 m) joint spacing.

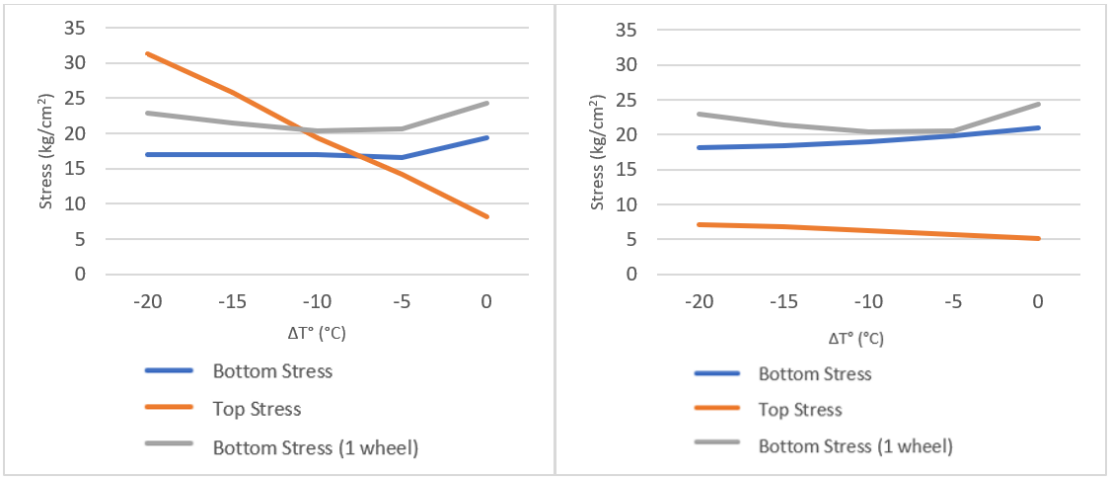

Figure 14, Stress vs ΔT° for traditional slabs and Stress vs ΔT° for short slabs

As seen in Figure 14, for the larger slab sizes, a change in the mode of failure occurs as the temperature gradient, and consequently, slab curl, increases. For a flatter slab and until the

internal temperature gradient is less than -9°F (-5°C), the maximum absolute stress occurs on the bottom of the slab. However, as the internal temperature gradient increases and the slab becomes increasingly curled, the maximum absolute stress then occurs on the top of the slab. However, Figure 14 indicates that when shorter slab lengths are considered, the absolute maximum stress always occurs at the bottom of the slab. These figures together indicate the effect of internal temperature gradient (built in slab curl) on the calculated stresses, and ultimately failure modes, for different slab sizes.

Real capacity of the Pavement System. In addition to the calculation of stresses in rigid pavements discussed in the previous section, material and shape dependent factors must be considered when calculating the full system of load effects on concrete. Full scale testing of pavements indicate that the maximum capacity of a pavement system is dependent on multiple factors, including the material properties of the concrete (concrete weight, fiber dosage), and the type and location of failure within the pavement system.

Therefore, a factor to describe the real capacity of the pavement system, SR, will be introduced. This factor is the quotient between the slab stress and the actual capacity of the pavement system, given its specific failure mode.

$$SR = \frac{\sigma}{MOR * C_1 * C_2} \tag{7}$$

Where:

$\boldsymbol{SR}$ = **Real capacity of the "Pavement System"**
$\boldsymbol{\sigma}$ = $Slab\ stress\ (kg/cm^2)$
$\boldsymbol{MOR}$ = $Concrete\ modulus\ of\ rupture$
$\boldsymbol{C_1}$ = $Slab/beam\ factor:\ C_1 = a * hpcc^2 + b * hpcc + c\ (Covarrubias\ 2007)$
$\boldsymbol{C_2}$ = $Structural\ fiber\ factor: C_1 = \frac{f_{150}^{150}}{MOR} * SF * a\ (Roesler\ et\ al)$
$\boldsymbol{a, b, c}$ = $Calibration\ factors$

Case 2.1 (Pavement system capacity in flat slabs):

The pavement system capacity was then calculated using Equation (7) and the previously calculated stress values for flat slabs, discussed in Case 1.1. The identical parameters were used for these calculations while including some additional material properties to calculate the SR. A plot of these SR factors as a function of joint spacing is given in Figure 15 below.

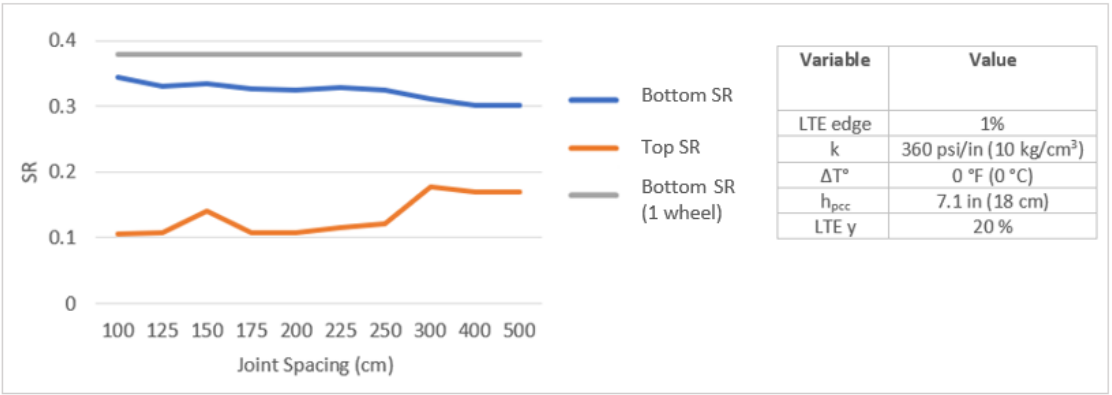

Figure 15, SR vs Joint Spacing in flat slabs

Figure 16 below compares the behavior of the SR and the calculated stresses in the pavement system. There trends between the SR and the calculated stresses with respect to slab thickness are very similar. It can also be seen that the maximum stresses on the bottom part of the slab are extremely sensitive to the slab thickness, more so than the maximum stresses on the top of the slab.

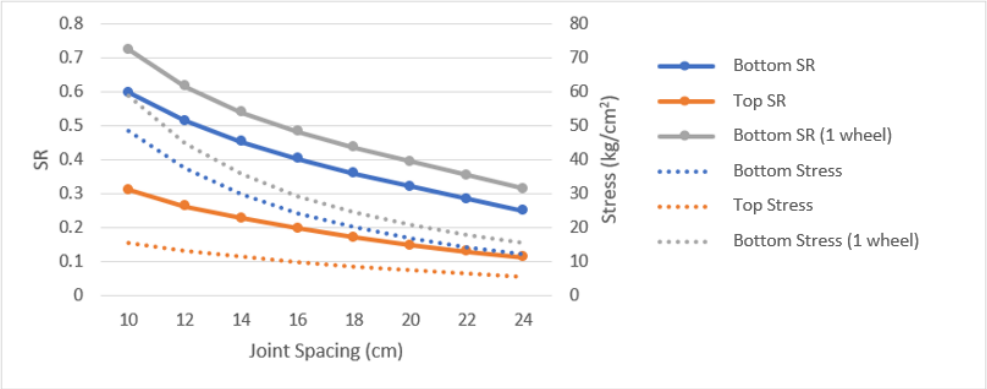

Figure 16, SR and Stresses vs slabs thickness

Figure 16 indicates that the stresses (plotted with dotted lines) increase at a higher rate than the SR (plotted with solid lines) for decreasing pavement thicknesses. This is due to the inclusion of the C1 factor, which increases the relative contribution of the subgrade support which increases the relative load capacity of the pavement system. However, this effect is not observed for the case of the maximum stresses and SR observed on the top of the slab.

Case 2.2 (Pavement system capacity, SR, with upward curling):

The SR was then calculated using Equation (7) and the previously calculated stress values for curled slabs, discussed in Case 1.2. The identical parameters were used for these calculations while including some additional material properties to calculate the SR. The curled slab was simulated by including an internal temperature gradient of -27°F (-15°C). Additionally, these stress results were compared to simulating FRC. A plot of these SR factors as a function of joint spacing is given in Figure 17.

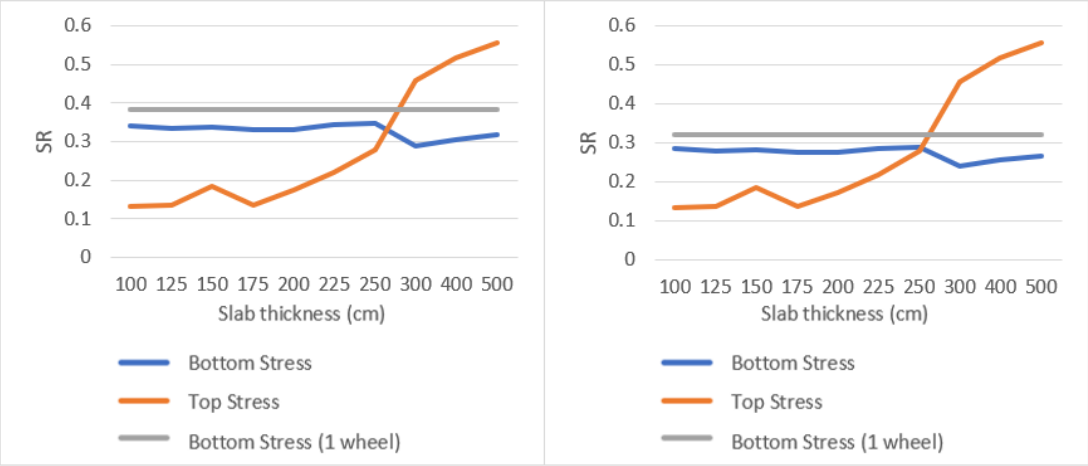

Figure 17, SR vs joint spacing with plain concrete vs FRC

It can be seen from Figure 17 that similar to the calculation of stresses for flat concrete pavements, the critical SR capacity for the top surface of the slab is seen to exceed the SR capacity for the bottom surface of the slab as the joint spacing increases.

Case 3.1 (Admissible traffic):

The previously calculated slab capacity can be used to quantify the pavement system capacity in terms of traffic. Equation (8) establishes a relationship between the ultimate number of admissible load repetitions (admissible load traffic), N, as a function of the SR ratio, previously calculated in Equation (7).

$$N = 2 * (SR)^{-1,22} \tag{8}$$

Where:

N = **Number of admissible loads for a condition**
SR = **Real capacity of the "Pavement System"**

The number of admissible repetitions can be taken as the minimum value between the calculated "pavement system" capacity for the top and bottom stresses, in order to obtain the number of admissible repetitions of the system in the entire slab, given in Equation (9).

$$N = min\ (N_{top}, N_{bottom}) \tag{9}$$

Where:

N = **Number of admissible loads for a condition from Equation (8).**
N_{top} = Number of admissible loads calculated from the top stresses with Equation (8).
N_{bottom} = Number of admissible loads calculated from the bottom stresses with Equation (8).

Using the same values as Case 2.2 to calculate the pavement system capacity of an upwardly curled slab, Figure 18 shows the admissible traffic for the maximum stresses from the top and bottom of the slab as well as the minimum number of load repetitions based on the minimum of either case (indicated by a dotted line).

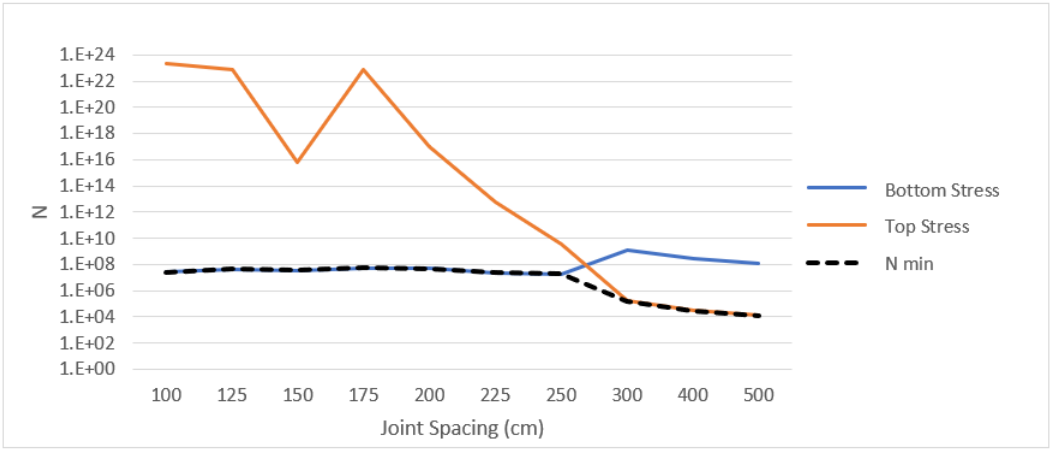

Figure 18, Admissible traffic vs joint spacing for different type of stresses, without fiber

Figure 18 has calculated this admissible traffic value when no fibers are included. However, the pavement system capacity calculation in Case 2.2, of the upwardly curled slab, indicated that there may be an increase in the capacity of the pavement system with respect to stresses on the bottom of the slab when fibers are included. Therefore, the same analysis was completed with fibers in the concrete mixtures, given in Figure 19 below.

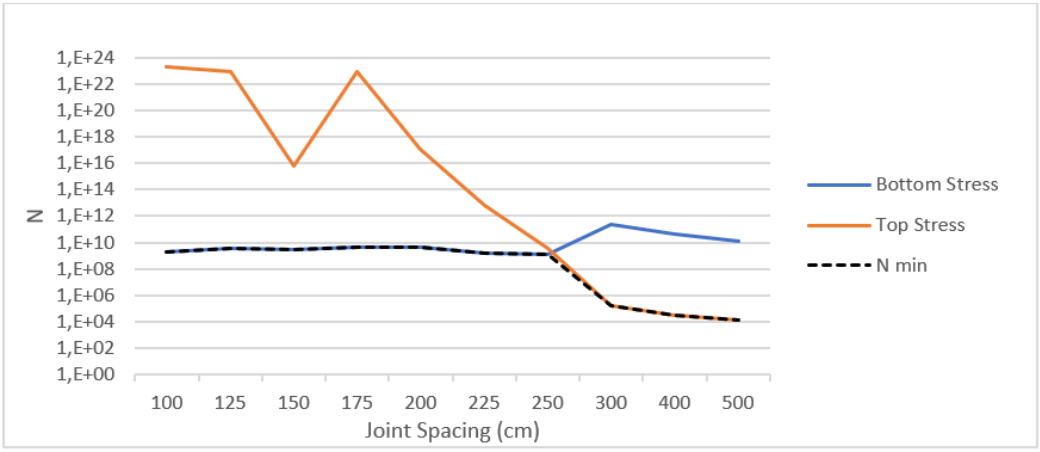

Figure 19, Admissible traffic vs joint spacing for different type of stresses, with fiber

It can be seen from Figure 19 that, when including fibers the admissible traffic increases for the number of load repetitions only when the slab is smaller than 8.2 ft (250 cm). There was no effect on the admissible traffic when the failure mode was controlled by stresses on the top of the slab.

The admissible traffic conditions (indicated in Figure 18 and Figure 19 by the black dotted line) can then be analyzed with different temperature gradients. The results of this comparison can be seen in Figure 20 without fibers below when plotted as a function of the joint spacing.

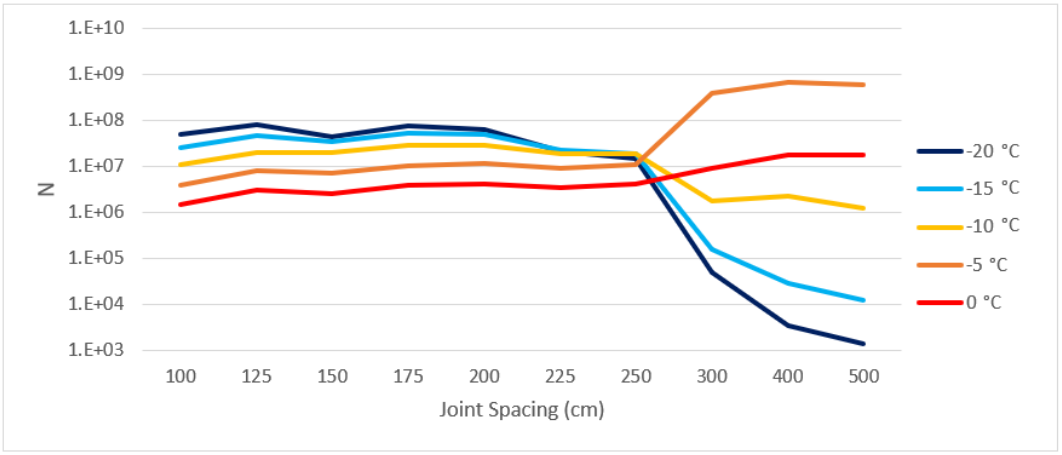

Figure 20, Admissible traffic vs joint spacing for different temperature gradients

Two primary observations can be made from Figure 20. The first is that the number of allowable load repetitions varies tremendously as a function of the temperature gradient of the slab for joint spacing between 8.2 ft and 16.4 ft (250 and 500 cm). However, for shorter

joint spacing, those between 3.3 and 8.2 ft (100 and 250 cm) have a consistent relationship where larger temperature gradients result in a higher number of admissible load repetitions in the studied case.

The first observation indicates variability in the number of admissible loads per the temperature gradient. This indicates the importance of the selection of slab gradient in a slab design, especially for slabs with a larger joint spacing.

The second phenomenon can be explained by the shape of the slab and the load interaction in each temperature gradient. A greater temperature gradient (more negative) indicates more concave slabs, with their edges raised and a smaller area of contact with the base. Because of this shape, compressive stresses are induced in the lower central part of the slab that are opposed to those generated by the loads.

When performing the same analysis, altering only the inclusion of fiber, the contribution of the fiber to the loading capacity of the pavement system can be seen in Figure 21. Again, the admissible load was calculated as function of joint spacing across several temperature gradients indicating different degrees of upward slab curl.

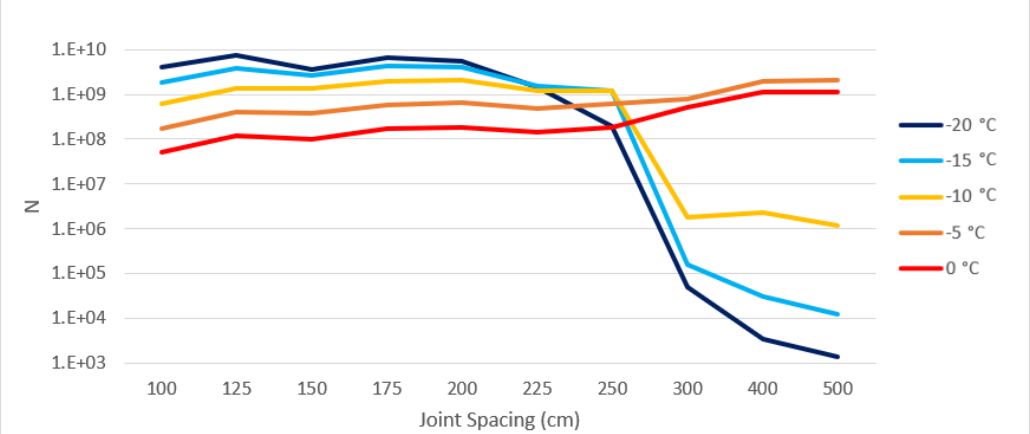

Figure 21, Admissible traffic vs joint spacing for different temperature gradients, FRC

Again, it can be seen from Figure 21 the addition of fiber in normal dosages, does not increase the real slab capacity in terms of traffic except for slabs with a very low temperature gradient (0°F or -9°F (0°C or -5°C) or small slab sizes, less than 8.2 ft (250 cm).

That said, it can be dangerous to use a methodology that only calculates stress at the bottom of the slabs and seeks to obtain a thickness optimization by including fiber in the concrete, when the methodology is not able to see what happens at the top of the slabs, which can control the design in terms of stresses in cases of curling and traditional slabs dimensions, delivering an inaccurate design,

Application to design cases

To compare differences between the design methods and the actual behavior of the slabs across different conditions while considering the interaction of relevant design variables, the results of two real designs will be discussed. Utilizing both AASHTO 93 and

PavementDesigner.org, sample pavement cases will be designed to evaluate and compare the structural behavior across different conditions with those considered intrinsically in the calibration of the model.

Evaluation of an AASHTO 93 pavement design. The AASHTO 93 method was used to design a large urban roadway located in Lima, Perú, and using certain input criteria recommended by the Portland Cement Association (PCA). The main design inputs were:

- Traffic: 8,070,000 ESALS
- Reliability: 80%
- MOR: 740 psi (5.1 MPa)
- Structural fiber (it was considered as a contribution to the value of MOR)
- Modulus of elasticity: 4,400,000 psi (30,375 MPa)
- Load transfer coefficient: 3
- Subgrade reaction modulus: 83.4 MPa/m
- Joint spacing: 9.8 ft (300 cm)
- Initial serviceability: 4.5
- Terminal serviceability: 2

Using these inputs with the AASHTO 93 method of design, a concrete pavement with a thickness of approximately 6.7 in (17 cm) is sufficient. (see Appendixes AASHTO 93 design inputs).

With the proposed structure and considering similar conditions to the calibration, SR ratio variability at the top and bottom of the slabs was calculated varying factors such as joint spacing, fiber inclusion, and temperature gradient, for both cases.

In the following graphs, a slab thickness of 7.1 in (18 cm) was used since the study carried out does not include 6.7 in (17 cm) as input. However, 7.1 in (18 cm) thick slabs will only be slightly more conservative. In addition, the effect of using FRC was included as in the following calculations, that is, as a structural contribution in the bottom of the slabs.

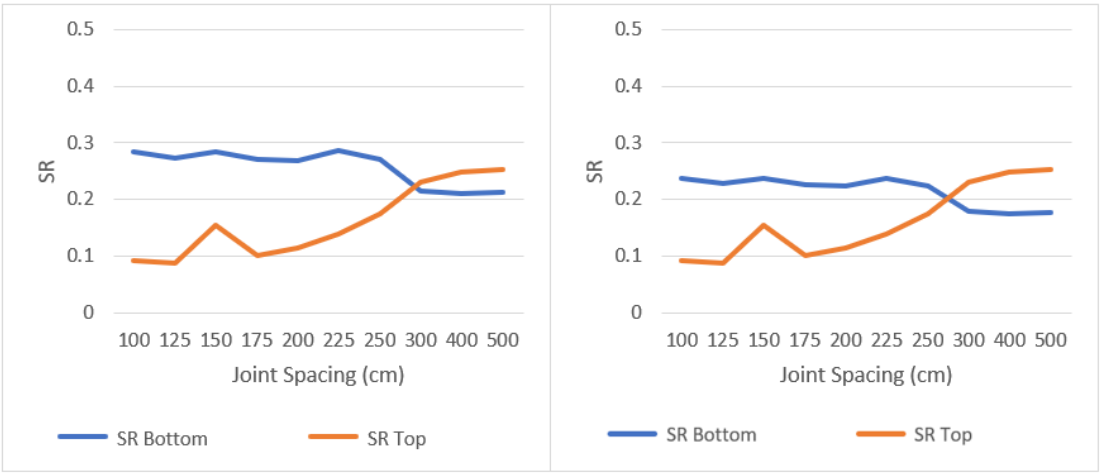

Figure 22, SR vs joint spacing, real case without and with fiber

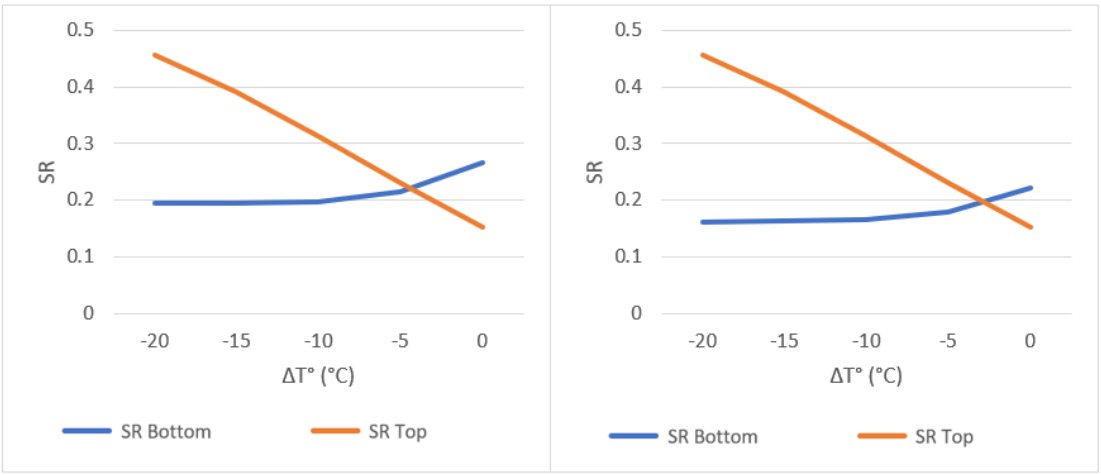

Figure 23, SR vs ΔT°, real case without and with fiber

Figure 24, calculated using the described inputs and intrinsic conditions assumed by AASHTO93 method (climate, curling, etc.) shows the number of admissible load repetitions of the system as a function of slab thickness for both plain and FRC. It can be seen that the inclusion of fiber increases structural capacity of the bottom part of the slab, because bottom up cracking is the controlling failure mode.

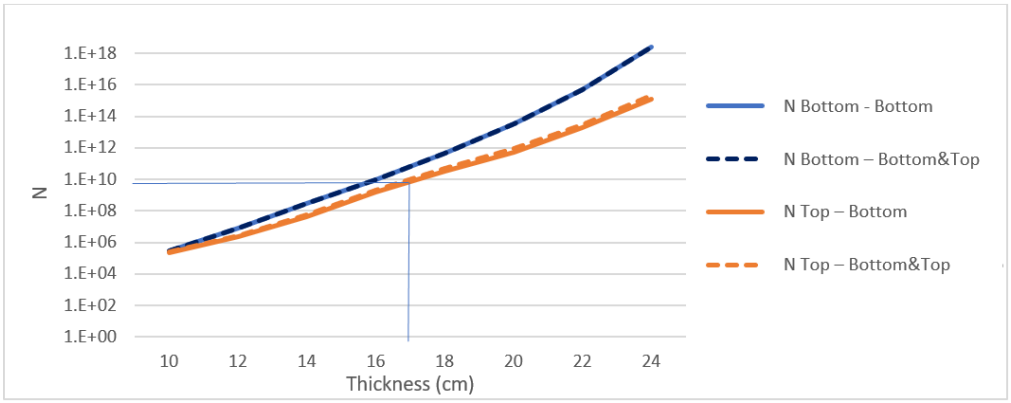

Figure 24, Admissible traffic vs slab thickness according to fiber effect (top or bottom)

Figure 24 indicates that as modeled in the actual design (plotted with dotted lines), a higher load repetition capacity at the top of the slabs is observed because fiber contributes to the tensile strength of the system. It should be noted that the vertical axis is logarithmic and therefore, the numerical differences are larger than by scale.

For the design conditions, the number of admissible load repetitions is limited by the capacity in the bottom part of the slab across all thicknesses. In Figure 25, a temperature gradient of -9°F (-5°C) was used, which is close to the temperature gradients measured in Illinois, where the AASHTO model was calibrated.

For a slab of approximately 6.7 in (17cm) thickness, there are about 1*E+10 admissible load repetitions, which can be considered practically infinite fatigue for this condition. It is important to note that this is not a design but rather a single example to provide a comparison between the admissible load repetitions for different design conditions.

The analysis can be repeated with the minimum of admissible load repetitions across different temperature gradients and subgrade reaction moduli. The results of this analysis are given in Figure 25:

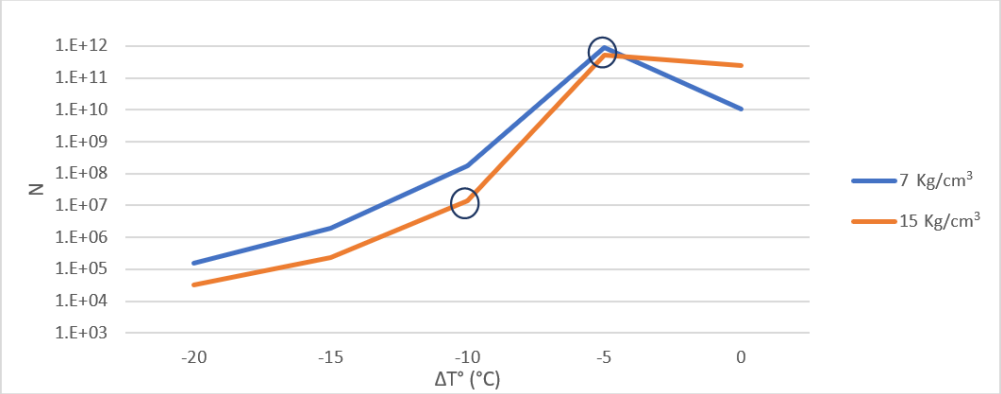

Figure 25, Admissible traffic vs ΔT° for different k-values, AASHTO 93 case

However changing soil properties or temperature gradient values substantially changes the stress. Therefore, actual experienced stresses can vary significantly from design values as these two variables can be more difficult to correctly estimate. When considering a temperature gradient of -27°F (-15°C), the designed pavement admits a very small number of load repetitions in comparison to the original design. Therefore, using design methods with local calibration constants that fail to address the unique conditions of a projects can be extremely unconservative. Similarly, using the AASHTO design method but including fiber changes the failure mode of the slab itself, but this change is not incorporated in design.

Pavement evaluated with PavementDesigner.org. Pavement Designer (PD), a pavement design software using design methods developed by the American Concrete Pavement Association (ACPA), Portland Cement Association (PCA), and the National Ready Mixed Concrete Association (NRMCA), was also used to calculate stresses in the given pavement system for the loading condition of a single wheel loading located at the pavement edge between two joints. The SR value does not vary significantly across different slab dimensions or temperature gradients, as seen in Figure 26 below.

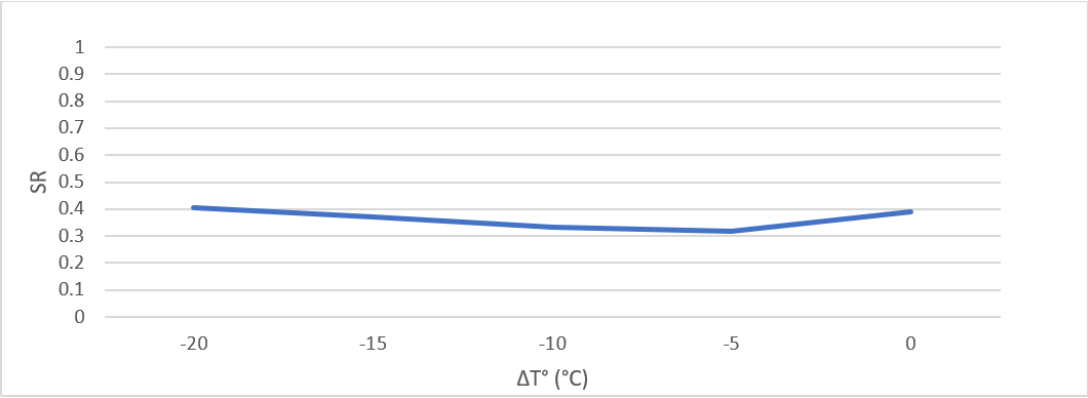

Figure 26, SR vs ΔT°(°C) for one Wheel at the edge, PD case

From this lack of SR variation, it is clear that the Pavement Designer method does not consider the temperature gradient as a design input value.

To evaluate a design with PavementDesigner.org, the following design input values were considered:

- Traffic: 500 trucks per day (Major Arterial, 4% growth per year)
- Reliability: 80%
- Percentage of slabs cracked at the end of the period: 20% (80%)
- MOR: 725 PSI
- Elasticity module: 4,206,094 PSI
- Edge support: No
- Base treated with cement: 500,000 PSI, 6 in
- K-value: 781 PSI/in

Thus, the software recommends a 7.25 inch (18.3 cm) thick pavement with 10 feet (3.0 m) joint spacing and no load transfer dowels, or 6.25 inches (15.9 cm) thick with 9 feet (2.7 m) joint spacing and load transfer dowels at the joints.

The case without dowels with respect to allowable traffic loading is given in Figure 27:

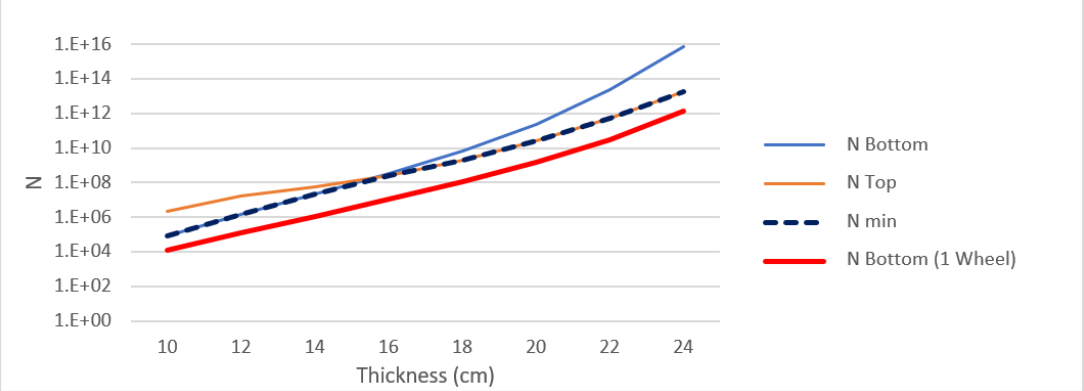

Figure 27, Admissible traffic vs slab thickness, PCA case

The above graph compares the number of admissible load repetitions for a full truck (dotted line) and a single wheel on the edge (red line) across different slab thicknesses, considering a temperature gradient of -9°F (-5°C), which resembles the local calibration conditions of the software. For the calculated configuration, about 10^8 load repetitions are allowed. The loading case of a single wheel is conservative, as the number of load repetitions for a full truck load is only slightly larger.

This design is theoretically applicable to any projected pavement with the chosen materials, support conditions and load repetitions. However, varying the project location will require inputting climate conditions that are different from those in the software calibration model. These climatic values; however, are unalterable because they are intrinsically incorporated into the model. The effect of altering temperature gradient is shown in Figure 28 for a slab with 7.1 in (18 cm) thickness:

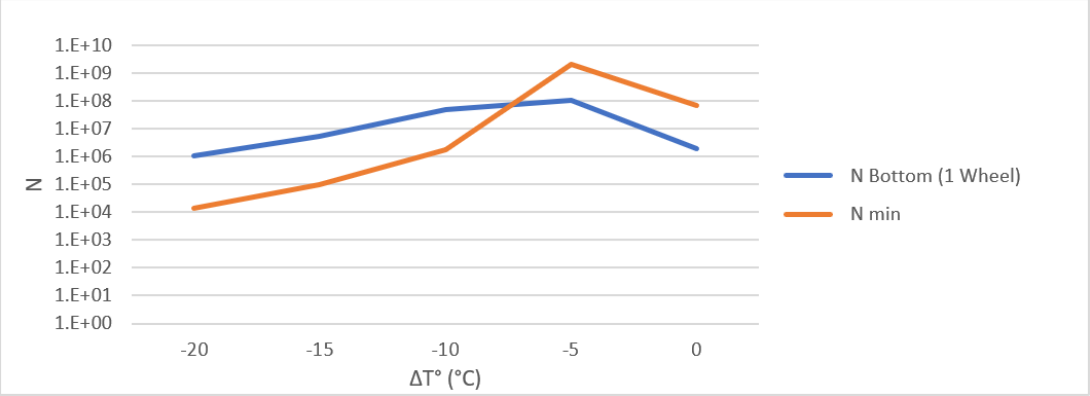

Figure 28, Admissible traffic vs temperature gradient, PCA case

Using a temperature gradient of -18°F (-10°C), considerable differences in the number of admissible load repetitions can be seen when considering a full truck on the pavement instead of loading only a single wheel at the edge. This observation suggests it may be risky to apply this methodology to the design of a pavement with different climatic conditions than those used in the software calibration model.

Conclusions

Current rigid pavement design methodologies are limited by the data sets from which they are calibrated. To extend variables beyond this inference space extends the design methodology beyond its intended scope and produces possibly incorrect solutions.

Concrete pavements contain relevant design variables that are often overlooked by different methodologies. However, many designers continue to use these methodologies, making adaptations and overlooking the complex interactions that exist within a pavement, which can hinder the development of a concrete pavement design methodology. Better solutions are available using finite element analysis tools, which better understand how a concrete pavement works under loads and different conditions.

The results presented in this paper are only cases that demonstrate the responses of each chosen condition in order, which serve to understand each situation and to make comparisons in terms of magnitude. In no case these results will serve to make a pavement design, given that this requires an iteration of variables considerably more complex than the one exposed, that compares different conditions and adds other variables that are not possible to synthesize in a work like this.

Currently there are more modern concrete pavements design methodologies than those used by many designers, which adjust better to the conditions of each project and correctly calculate the different failure modes and new materials properties.

Bibliography

AASHTO (1993) *Guide for Design of Pavement Structures,* American Association of State Highway and Transportation Officials, USA.

American Concrete Pavement Association (2012) *StreetPave12 Structural Design Software for Street and Road Concrete Pavements*, USA.

American Concrete Pavement Association (2018) *PavementDesigner.org*., USA.

ARA, Inc. (2007) *Interim Mechanistic-Empirical Pavement Design Guide Manual of Practice,* Final Draft, National Cooperative Highway Research Program Project 1-37A, USA.

ASTM International (2012) *ASTM C1550-12a, Standard Test Method for Flexural Toughness of Fiber Reinforced Concrete (Using Centrally Loaded Round Panel),* West Conshohocken, USA.

ASTM International (2019) *ASTM C1609 / C1609M-19, Standard Test Method for Flexural Performance of Fiber-Reinforced Concrete (Using Beam With Third-Point Loading),* West Conshohocken, USA.

Bordelon, A., Roesler, J.R. and Hiller, J.E. (2009) *Mechanistic-Empirical Design Concepts for Jointed Plain Concrete Pavements in Illinois*, Final Report, FHWA-ICT-09-052, Illinois Center for Transportation, University of Illinois, Urbana, USA.

Carmona, S. and Molins, C. (2019) *Use of BCN test for controlling tension capacity of fiber reinforced shotcrete in mining works*, Construction and Building Materials.

Covarrubias, J. P., Roesler, J., Roco, V. and Binder, C. E. (2012) *Effect of Built-in Curling on Concrete Pavement Performance and Design in Chile*, 10th International Conference on Concrete Pavements, International Society for Concrete Pavements, Canada.

ERES CONSULTANTS (1999) *ISLAB 2000, Finite Element Program for the Analysis of Rigid Pavements*, Version 1.1, USA.

Highway Research Board (1962) *The AASHO Road Test*, Report 7, Summary Report, NAS-NRC Division of Engineering and Industrial Research, USA.

Portland Cement Association (1984) *The Design for Concrete Highway and Street Pavements*, PCA, Skokie, U.S.A.

Rodden, R. et al Rodden, R., Voigt, G., and Wathne, L. (2014) *Comparison of Roadway Jointed Plain Concrete Pavement (JPCP) Thickness Design Methods Common in the United States (U.S.*), 12th International Symposium on Concrete Roads, Czech Republic.

Roesler, J. R. (2007) *Design and Specification of Concrete Pavements with Structural Fibers,* International Workshop on Best Practices for Concrete Pavements, USA.

TCPavements (2012) *Documentation and Design Guide OptiPave2®*, OptiPave2 Documentation, Chile.

TRB, (2007) *Pavement lessons learned from the AASHO road test and performance of the interstate highway system*, Transportation Research Board of the National Academies, USA.

Valenzuela, M. (2010) *Estudio del Comportamiento de Hormigones con Fibras Estructurales en Pavimentos*, Chile.

Appendixes

AASHTO 93 design inputs

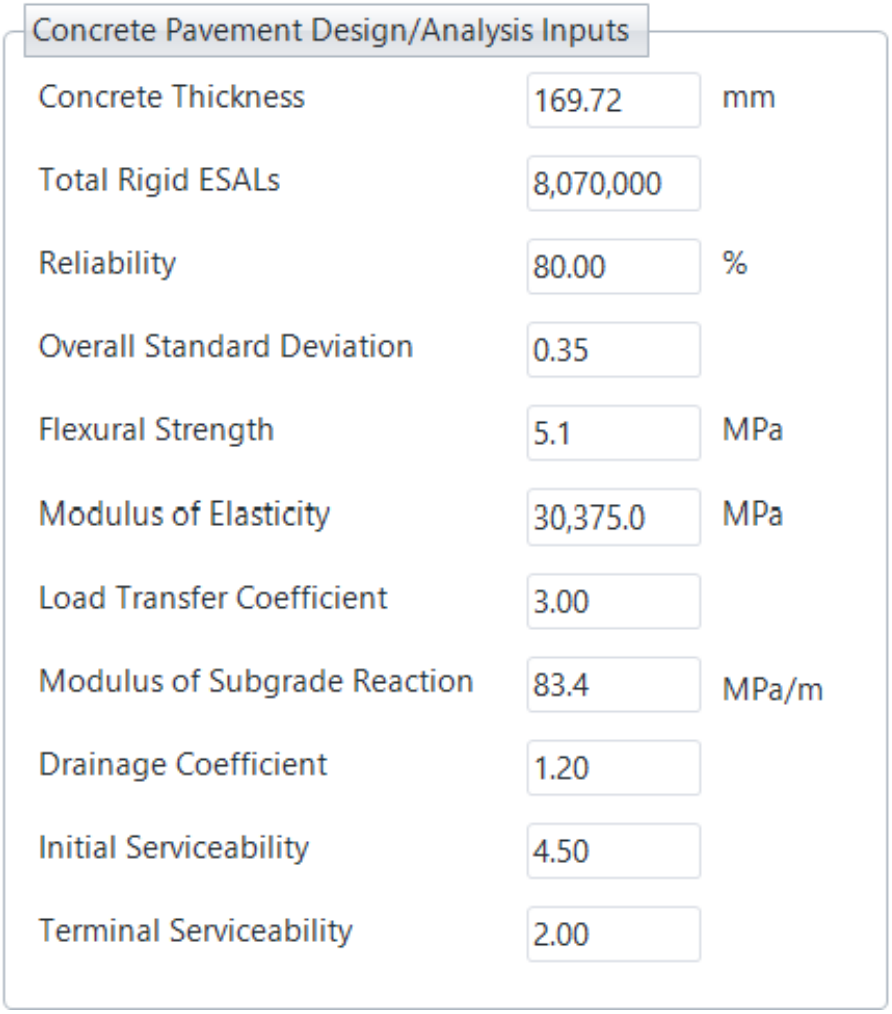

PavementDesigner Report

PavementDesigner.org

DESIGN SUMMARY REPORT FOR

JOINTED-PLAIN CONCRETE PAVEMENT (JPCP)

DATE CREATED:

Wed Oct 24 2018 11:25:32 GMT-0300 (hora de verano de Chile)

Project Description

Project Name: PD Test **Owner:** **Zip Code:**

Designer's Name: **Route:**

Project Description:

Design Summary

	Doweled	Undoweled		Doweled	Undoweled
Recommended Design Thickness:	6.25 in.	7.25 in.	Maximum Joint Spacing:	9 ft.	10 ft.
Calculated Minimum Thickness:	6.13 in.	7.12 in.			

Pavement Structure

SUBBASE

Calculated Composite K-Value of Substructure: 781 psi/in

Layer Type	Resilient Modulus	Layer Thickness
JOINTED PLAIN CONCRETE SURFACE		
Cement-Treated Base (CTB)	500,000 psi	6 in
SUBGRADE		

CONCRETE

28-Day Flex Strength: 725 psi
Modulus of Elasticity: 4206094 psi
Edge Support: No
Macrofibers in Concrete: No

SUBGRADE

CBR: 10 %
Calculated MRSG Value 9.389 psi

Project Level

TRAFFIC

Spectrum Type: Major Arterial
Design Life: 20 years

USER DEFINED TRAFFIC

Trucks Per Day: 500
Traffic Growth Rate %: 4 % per year
Directional Distribution: 100 %
Design Lane Distribution: 100 %

GLOBAL

Reliability: 80 %
% Slabs Cracked at End of Design Life: 20 %

Avg Trucks/Day in Design Lane Over the Design Life: 744
Total Trucks in Design Lane Over the Design Life: 5.438.222

Design Method

The PCA design methodology from StreetPave, was used to produce these results.

PavementDesigner.org

DESIGN SUMMARY REPORT FOR

JOINTED-PLAIN CONCRETE PAVEMENT (JPCP)

DATE CREATED:

Wed Oct 24 2018 11:26:53 GMT-0300 (hora de verano de Chile)

Project Description

Project Name: PD Test frc **Owner:** **Zip Code:**

Designer's Name: **Route:**

Project Description:

Design Summary

	Doweled	Undoweled		Doweled	Undoweled
Recommended Design Thickness:	5.75 in.	7.25 in.	Maximum Joint Spacing:	8 ft.	9 ft.
Calculated Minimum Thickness:	5.75 in.	7.06 in.			

Pavement Structure

SUBBASE

Calculated Composite K-Value of Substructure: 781 psi/in

Layer Type	Resilient Modulus	Layer Thickness
JOINTED PLAIN CONCRETE SURFACE		
Cement-Treated Base (CTB)	500,000 psi	6 in
SUBGRADE		

CONCRETE

28-Day Flex Strength:	725 psi	Edge Support:	No
Modulus of Elasticity:	4206094 psi	Macrofibers in Concrete:	Yes

SUBGRADE

CBR:	10 %
Calculated MRSG Value	9.389 psi

Project Level

TRAFFIC

Spectrum Type:	Major Arterial
Design Life:	20 years

USER DEFINED TRAFFIC

Trucks Per Day:	500
Traffic Growth Rate %:	4 % per year
Directional Distribution:	100 %
Design Lane Distribution:	100 %

GLOBAL

Reliability:	80 %
% Slabs Cracked at End of Design Life:	20 %

Avg Trucks/Day in Design Lane Over the Design Life:	744
Total Trucks in Design Lane Over the Design Life:	5.438.222

Design Method

The PCA design methodology from StreetPave, was used to produce these results.